

Environmental vs demographic variability in stochastic predator-prey models

U Dobramysl and U C Täuber

Department of Physics, Virginia Tech, Blacksburg, Virginia 24061-0435, USA

E-mail: ulrich.dobramysl@vt.edu, tauber@vt.edu

Abstract. In contrast to the neutral population cycles of the deterministic mean-field Lotka–Volterra rate equations, including spatial structure and stochastic noise in models for predator-prey interactions yields complex spatio-temporal structures associated with long-lived erratic population oscillations. Environmental variability in the form of quenched spatial randomness in the predation rates results in more localized activity patches. Population fluctuations in rare favorable regions in turn cause a remarkable increase in the asymptotic densities of both predators and prey [1]. Very intriguing features are found when variable interaction rates are affixed to individual particles rather than lattice sites. Stochastic dynamics with demographic variability in conjunction with inheritable predation efficiencies generate non-trivial time evolution for the predation rate distributions, yet with overall essentially neutral optimization [2].

PACS numbers: 87.23.Cc, 05.40.-a, 87.18.Tt

Keywords:

- Population dynamics (Theory)
- Models for evolution (Theory)
- Mutational and evolutionary processes (Theory)
- Stochastic particle dynamics (Theory)

Submitted to: *J. Stat. Mech. Theor. Exp.*

1. Introduction

1.1. Ecology and Population Dynamics

The field of population dynamics deals with the mathematical modeling of interacting species. It has been a very active field since about 40 years [3, 4, 5, 6] and continues to provide exciting challenges. Ecological environments are complicated systems with many participating agents, fluxes of energy and resources and many inputs and outputs. There also exists a wealth of different models for various applications. The ecological

dynamics of three, cyclically competing species of californian lizards can be modeled using the rock-paper-scissors model [7, 8]. In the case of highly asymmetric interaction rates, the three species rock-paper-scissors model can be mapped to the two-species Lotka-Volterra model [9]. The cyclic competition between four and more species has also been extensively studied [10, 11, 12, 13].

Here, we focus on the Lotka-Volterra (LV) model, independently introduced in 1920 by A. J. Lotka [14], and by V. Volterra in 1926 [15]. The LV model consists of two species, the predator species A and the prey species B , obeying the following three rules:

$$A \xrightarrow{\mu} \emptyset, \tag{1a}$$

$$B \xrightarrow{\sigma} 2B, \tag{1b}$$

$$A + B \xrightarrow{\lambda} 2A. \tag{1c}$$

Rule (1a) governs predator mortality, on its own leading to an exponential decay of the predator population with a characteristic rate μ . Rule (1b) represents prey reproduction and leads to an exponential increase in the number of prey with rate σ in the absence of any controlling processes, such as predation or the introduction of finite carrying capacities (i.e. restrictions on the global or local population size). Rule (1c) finally introduces predator-prey interaction, wherein a prey particle is consumed by a predator with a predation rate λ and simultaneously a new predator particle is created. Hence, the only way the predator population can be sustained (or grow) is by consuming prey, which is also the only way the prey population can be kept from growing indefinitely. The simplicity of the LV model obviously leads to a limited applicability to real ecological predator-prey systems:

- The prey population reproduces at a constant rate, which implies that growth is not limited by the availability of food resources of this species.
- The mortality of single predators is uniform and does not depend on the abundance of prey.
- Natural processes that might lead to prey death occur on much larger time scales than the predation interaction, hence they are negligible. This is probably justified as long as both species coexist. In the event of predator extinction or near-extinction this assumption might yield unnatural results.
- Predator reproduction is directly coupled to predation. While it is reasonable to assume a connection between the reproduction rate of a predator species and the availability of food, a direct conversion of prey to predator is too simple.

This list is by no means exhaustive. A more thorough criticism of the LV model can be found in reference [16]. We nevertheless find the LV-model to be a useful tool and a good starting point for the study of variability, especially due to its minimal set of rules.

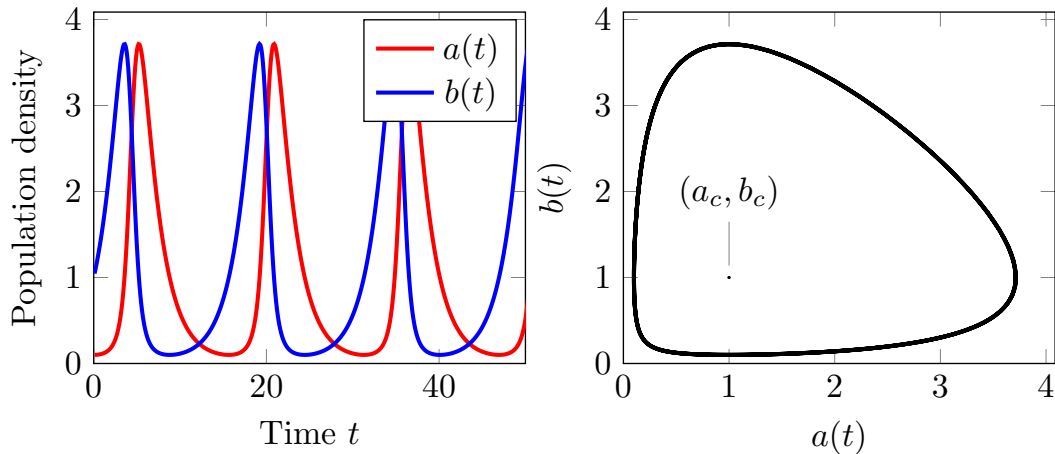


Figure 1. LV mean-field oscillations and phase space trajectory. The LV mean-field rate equations (2) give rise to nonlinear oscillations around the coexistence fixed point $(\sigma/\lambda, \mu/\lambda)$. The left panel shows the predator and prey population densities $a(t)$ and $b(t)$ as a function of time t for the reaction probabilities $\sigma/\tau = 0.5$, $\mu/\tau = 0.5$ and $\lambda/\tau = 0.5$ (τ indicates unit time) and initial densities of $a(0) = 0.1$ and $b(0) = 1$. The oscillations are clearly visible. The right panel displays the phase space trajectory as a closed cycle around the coexistence fixed point.

1.2. Mean-Field Rate Equations

In order to construct the mean-field rate equations for the LV model (1) one assumes that the populations of both species are well-mixed and distributed homogeneously, such that one can ignore spatial and temporal correlations and fluctuations. Since the predator population decreases exponentially with rate μ , the change of the predator population has to include the term $-\mu a(t)$, where $a(t)$ denotes the time-dependent spatially averaged density of species A . Similarly, the prey population density $b(t)$ increases exponentially with a rate σ , hence its first derivative must include the term $\sigma b(t)$. The predation interaction depends on the availability of both predators and prey, hence the interaction term has to depend on both densities and the predation rate λ . The interaction is conservative in the sense that one prey is converted into exactly one predator, thus the mean-field (mass action) factorization of the interaction term $\lambda a(t)b(t)$ enters positively and negatively into the predator and prey density change, respectively. Putting everything together yields the LV mean-field rate equations:

$$\frac{da(t)}{dt} = \lambda a(t)b(t) - \mu a(t) , \quad (2a)$$

$$\frac{db(t)}{dt} = \sigma b(t) - \lambda a(t)b(t) . \quad (2b)$$

These equations may be derived in a more formal manner via the master equation of the LV model (4) (for the detailed procedure see section 1.3 below and reference [17]).

By setting the left-hand side of equations (2a) and (2b) to zero, one immediately finds the fixed points of this system with stationary densities (a_{fp}, b_{fp}) :

- (i) The trivial fixed point where both population densities are zero $(0, 0)$.
- (ii) The predator extinction fixed point, with the prey population tending to infinity $(0, \infty)$.
- (iii) The species coexistence fixed point where both predator and prey densities are finite $(a_c = \sigma/\lambda, b_c = \mu/\lambda)$.

The trivial and the predator extinction fixed points are both linearly unstable with respect to small perturbations in the densities a and b (with $\lambda = 0$ the state $(0, \infty)$ becomes stable). The coexistence fixed point is marginally stable: linear stability analysis yields purely imaginary eigenvalues, hence this fixed point gives rise to marginal population cycles. This is the origin of the characteristic LV oscillations, displayed in figure 1; in the limit of small amplitudes, the linear oscillation frequency is $\omega = \sqrt{\mu\sigma}$. These stable phase space orbits are associated with a first integral of motion of the LV mean-field rate equations. By dividing equations (2a) and (2b) and separating the variables we get

$$\left(\frac{\sigma}{a} - \lambda\right) da = \left(-\frac{\mu}{b} + \lambda\right) db .$$

Integrating both sides yields the constant expression

$$K(t) = \sigma \ln a(t) + \mu \ln b(t) - \lambda[a(t) + b(t)] = K(0) , \quad (3)$$

which is also the Lyapunov function of the LV system. A rigorous stability analysis of the LV mean-field equations can be found in references [18, 19].

1.3. Stochasticity and Simulations

The derivation of the mean-field equations discussed in the last section assumes that the system is well-mixed and deterministic. This assumption is in general not valid for ecological systems, which are stochastic in nature. Hence, we numerically solve the underlying master equation using Monte Carlo simulations. Via a rescaling with an appropriate unit of time we obtain the single-particle probabilities from the rates μ , σ and λ . The master equation of the LV system with parallel and independent updates reads:

$$\begin{aligned} \frac{dP(A, B, t)}{dt} = & \mu(A+1)P(A+1, B, t) + \sigma(B-1)P(A, B-1, t) \\ & + \lambda(A-1)(B+1)P(A-1, B+1, t) - (\mu A + \sigma B + \lambda AB)P(A, B, t) , \end{aligned} \quad (4)$$

where $P(A, B, t)$ denotes the probability of the system being in a state with A predator and B prey particles at time t . By solving equation (4) for $dP/dt = 0$ one finds that this system has exactly one steady-state solution, namely $P(A = 0, B = 0, t \rightarrow \infty) = 1$ and $P(A > 0, B > 0, t \rightarrow \infty) = 0$ [20]. Hence, the previously unstable trivial extinction fixed point becomes a stable absorbing state. Due to the discrete nature of the stochastic system, fluctuations in the number of particles can drive the population into extinction

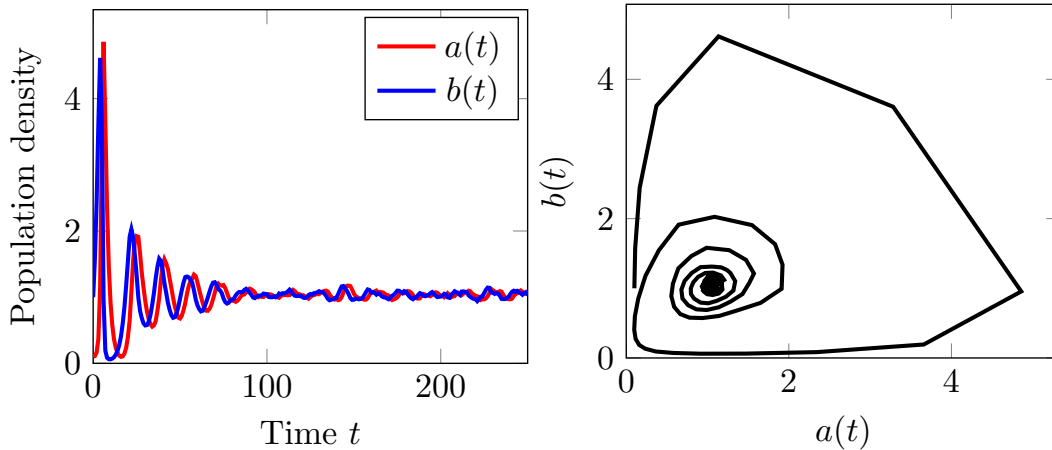


Figure 2. Population densities from a single Monte Carlo simulation run. The left panel shows the predator and prey densities $a(t)$ and $b(t)$ as functions of time t for $\sigma = 0.5$, $\mu = 0.5$, and $\lambda = 0.5$, with initial densities $a(0) = 0.1$ and $b(0) = 1$. One can clearly see that the LV oscillations are now damped due to the stochastic nature of the simulation; the densities approach the coexistence fixed point. After reaching the steady state the densities perform erratic oscillations around these values driven by population number fluctuations. The right panel shows that the phase space trajectory of the simulation run is a spiral beginning at the initial densities of $(0.1, 1)$ and approaching the fixed point $(1 + \epsilon_a, 1 + \epsilon_b)$. The deviations ϵ_a and ϵ_b stem from a renormalization of the mean-field steady-state densities due to fluctuations.

if the number of particles becomes small. Moreover, this result implies that any system with a finite number of particles *always* reaches the extinction state, but the extinction time scale can become quite large already for reasonably sized systems [21]. This feature is absent in the mean-field rate equations since the population densities can get arbitrarily small without the population going extinct. The marginally stable species coexistence fixed point in the mean-field model becomes metastable in a stochastic system. While fluctuations will eventually drive the system to extinction, the coexistence state is long-lived. In Monte Carlo simulations, the population densities approach the coexistence densities via damped oscillations starting from the initial conditions. Figure 2 shows the species densities over time and the resulting spiral in phase space for a representative simulation run. Population fluctuations lead to small oscillations around the steady-state densities after the system reached the stationary state. Internal white noise stemming from the demographic stochasticity excites the resonant frequency of the system and results in these small oscillations. This leads to a drastic delay in the ultimate extinction of the system [22].

By introducing the mean particle densities as

$$a(t) = \sum_{A,B=0}^{\infty} AP(A, B, t) \quad \text{and} \quad b(t) = \sum_{A,B=0}^{\infty} BP(A, B, t),$$

we can derive the mean-field rate equations (2). Taking the time derivative of the mean

predator density and inserting the master equation (4) yields

$$\begin{aligned}
 \frac{da(t)}{dt} &= \sum_{A,B=0}^{\infty} A \frac{d}{dt} P(A, B, t) \\
 &= \sum_{A,B=0}^{\infty} [\mu A(A+1)P(A+1, B, t) + \sigma A(B-1)P(A, B-1, t) \\
 &\quad + \lambda A(A-1)(B+1)P(A, B, t) - (\mu A + \sigma B + \lambda AB)AP(A, B, t)] \\
 &= \sum_{A,B=0}^{\infty} [-\mu A + \lambda AB]P(A, B, t) ,
 \end{aligned}$$

where we shifted the summations over A and B in the last step. In order to arrive at the mean-field rate equation, we need to make the approximation that the probability to be in a state described by the particle numbers A and B factorizes into the independent probabilities of having A predators and B prey, $P(A, B, t) \approx P(A, t)P(B, t)$. This leads to

$$\frac{da(t)}{dt} \approx -\mu a(t) + \lambda a(t)b(t) ,$$

which is identical to the mean-field rate equation for the predator population (2a). An analogous derivation yields the rate equation describing the prey population (2b).

1.4. Spatial Structure

Ecological systems exhibit spatial structure. Members of species move through the environment foraging or evading predators. This leads to spatial correlations in the abundance of species, and emerging spatial patterns such as spirals or wavefronts [5, 8, 23, 24]. None of these features are captured by a mean-field model or by zero-dimensional stochastic models. It is however sometimes possible to use a stochastic PDE model to describe spatial patterns [25]. In Monte Carlo simulations in an ecological context, one generally uses a simple hyper-cubic lattice of edge length L and dimensionality d to introduce spatial structure. It is assumed that a simple diffusion process is adequate to describe the movement of species through space. Hence, particles hop from one lattice site to a randomly chosen neighboring site, performing random walks. A remarkable feature of the LV model is that the results in the coexistence phase are qualitatively independent of the details of the simulation method [18, 19, 26]. Yet it should be noted that the introduction of global or local population number restrictions induces a predator extinction threshold, separating the two-species coexistence phase from a state with proliferating prey filling the entire system. For the predator population this phase represents an inactive, absorbing state. Throughout this article, the number of particles is essentially unrestricted (up to a safety limit that is never reached in our simulations), hence this phase does not exist in our models.

Figure 3 shows representative snapshots from a one-dimensional and a two-dimensional LV Monte Carlo simulation. The one-dimensional simulation (left-hand

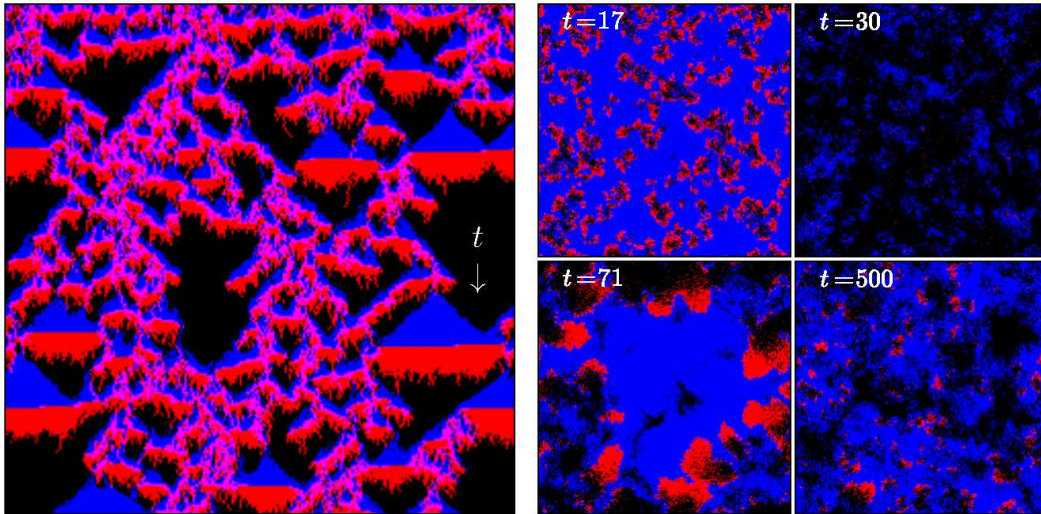


Figure 3. Snapshots from a one-dimensional and a two-dimensional spatial LV Monte Carlo simulation run. The left panel shows a one-dimensional simulation with $L = 250$, $\mu = 0.5$, $\sigma = 0.5$ and $\lambda = 0.3$, and initial densities $a(0) = 1 = b(0)$. The vertical direction shows time evolution while the horizontal is the spatial direction. The colors blue and red indicate the presence of prey and predator particles respectively, while a black pixel indicates an empty site. At $t = 0$ the system is still well-mixed and clusters of prey particles form and grow over time. Predators invade prey clusters and thereby often remove them completely. The right panel displays several snapshots from a two-dimensional simulation with $L = 250$, $\mu = 0.9$, $\sigma = 0.1$, and $\lambda = 1$. In the initial configuration, particles were randomly distributed with densities $a(0) = 0.01$ and $b(0) = 1$. The predator-prey community survives an initial predator invasion ($t = 17$), which leads to a subsequent prey proliferation due to predator scarcity ($t = 30$). Predator fronts start to invade a large prey cluster ($t = 71$). After the initial transient oscillations, the system reaches the coexistence quasi-steady state characterized by smaller prey clusters and predator invasion fronts ($t = 500$).

panel) progresses by forming prey clusters that are subsequently invaded by predators, which leads to intriguing spatio-temporal patterns. In the two-dimensional simulation, patches of prey particles form and become invaded by predators. Initially several large clusters span the system, which yields the observed synchronized oscillations in the densities. As the simulations progress the clusters become smaller and more numerous, hence the invasion cluster growth cycles de-synchronize throughout the lattice and the quasi-steady state is reached. The right-hand side of figure 3 shows several snapshots from a representative simulation run.

The remainder of this paper is structured in the following way: In the next section, we set the stage by briefly summarizing our findings on environmental variability in the interaction rates. In section 3, we discuss a non-spatial stochastic model for demographic variability and introduce our approximate mean-field description. We also compare the non-spatial model with results from two-dimensional simulations. In section 4, we investigate the full spatial system which includes both environmental and demographic variability. We finally conclude with section 5.

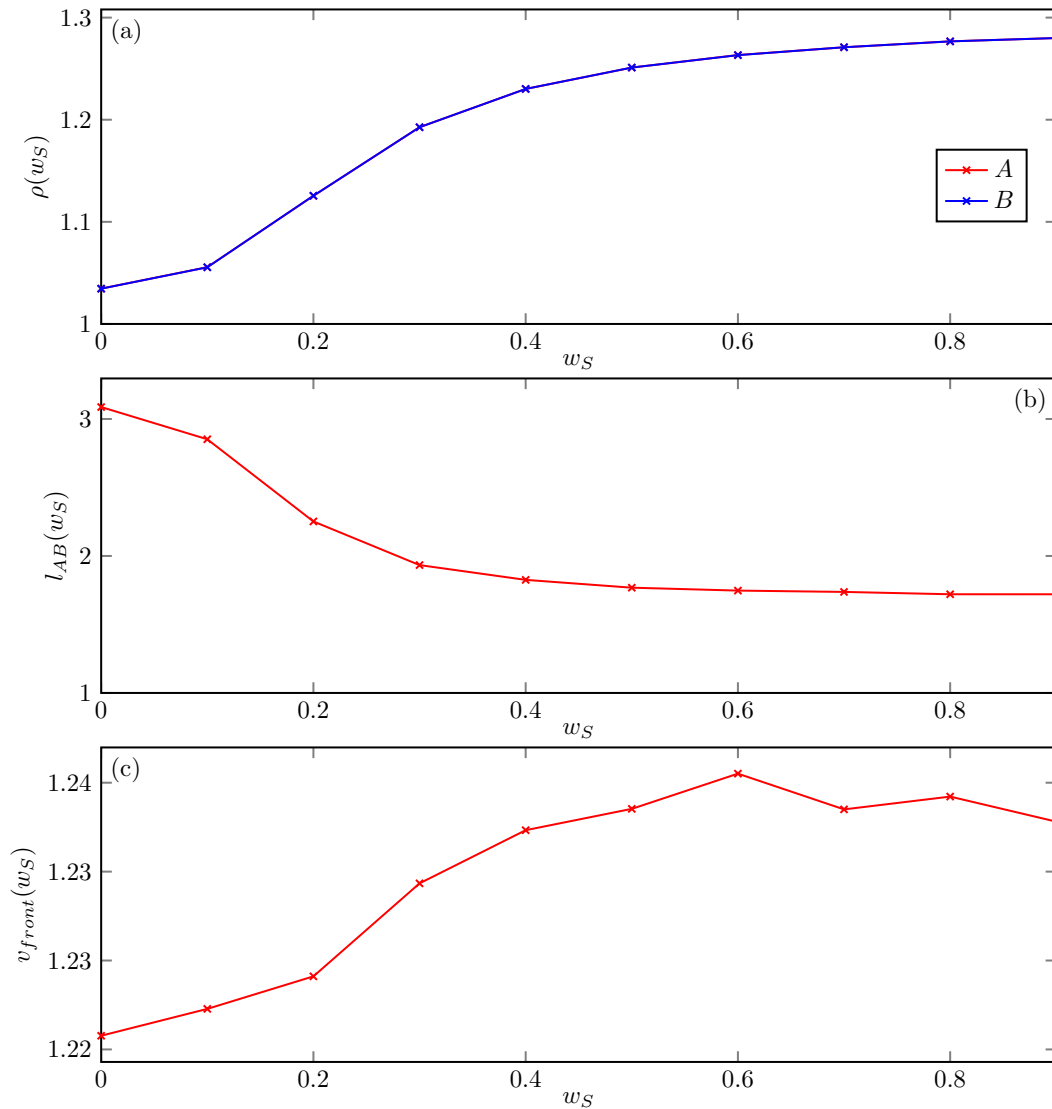


Figure 4. Effects of environmental variability. (a) The predator and prey species densities are enhanced by up to 24%, as a function of the variability w_S . (b) The typical distance between predator and prey particles decreases with increasing variability. (c) The speed of traveling wavefronts is enhanced as well. Data in this figure are taken from reference [1].

2. Environmental Variability

Ecological systems are in general not homogeneous. The availability of energy and resources can vary significantly over various length scales. In most ecological models, the effects of environmental variability are assumed to only enter via a trivial renormalization of the coarse-grained reaction rates. However, if the variation takes place on a similar length scale as the interactions, its effects are not adequately captured by such a simplified description. Hence, in our spatial ecosystem model, we choose to describe spatial variability by making the reaction rates spatially distributed quenched

random variables, subject to a Gaussian probability distribution, truncated to the interval $[0, 1]$, with mean $\frac{1}{2}$ and standard deviation w_S . This standard deviation is a measure of the amount of environmental variability and is thus a model parameter. More details about the implementation are given in reference [1].

Our previous work on this model confirmed the crucial role of environmental variability on the particle abundance. We found that the densities of *both* predator and prey species increase by up to 24% as a function of the variation strength; see figure 4(a). Other quantities are affected as well: e.g., the relaxation time to reach the quasi-steady state and the correlation lengths for either species as well as their typical separation distance become reduced with increasing disorder variance. This led us to conclude that the overall population increase was caused by more narrowly localized activity patches in which prey proliferate and predators feed off the out-diffusing prey; c.f. figure 4(b). Variability in the other rates μ and σ did not lead to significant changes in the system; see reference [1] for a detailed discussion. In our investigation, we also measured the speed of traveling activity fronts v_{front} (i.e. the fronts formed by a predator species invading a prey population). We found a small but significant enhancement of this quantity; see figure 4(c).

Environmental variability has also been subsequently investigated in the context of cyclic models, particularly the three species rock-paper-scissors and May-Leonard models. The effects of spatial variations in the reaction rates on both of these models were surprisingly small, which indicates that cyclic three-species models seem to be robust against the introduction of environmental variability [7, 24]. The macroscopic properties of these systems are hardly modified by stochastic fluctuations in general.

3. Demographic Variability

Variability can also be considered in the context of variation between individual members of each species. Due to differences in genetic heritage and learned strategies, the effectiveness with respect to reproduction, death, predation, etc. can vary between individuals of the same species. Hence, we may view the efficiency at certain processes as properties or traits of individual agents when modeling these systems. We focus again on the non-linear predation process and render the predation rate of a particular interaction between a predator and a prey particle a function of their respective predation efficacies.

The investigation of individual or demographic variability directly leads into a discussion of population-level evolution and optimization of traits. It is reasonable to assume that offspring inherit certain abilities from their parents. These abilities can be derived from the genetic make-up that is inherited from the parent generation, or they could also be strategies for food gathering or hunting patterns, learned through imitation from their immediate social surroundings. A combination of these determines a particular individual's efficiency at a given process, whence the more discrete nature of the genetic make-up and the presence or absence of certain strategies is smeared out. This coarse-grained interpretation of process efficiencies finally allows us to assume

that the efficacy value of a given offspring particle will be situated in the vicinity of its parent's. The severity of genetic mutations as well as the accuracy of strategy imitation between generations then determines the amount of inheritance variability of the coarse-grained efficiencies. Applied to the previously introduced LV system, this scheme allows for specific optimization of predation efficacies at the level of species populations, as discussed in subsection 3.3.

Optimization and evolution in predator-prey systems has been studied previously in experimental and theoretical contexts, by means of different models: Kishida *et al.* investigated reciprocal phenotype plasticity in salamanders and its tadpole prey. The gape of the salamander species adapted as a function of the body size of the tadpoles [27]. Yoshida *et al.* studied prey evolution in an experimental model using planktonic rotifers, and modeled this system using a system of nonlinear differential equations [28]. Fort and Inchausti employed an agent-based model that included a niche axis to study the emergence of biodiversity [29]. Rogers *et al.* designed a niche model and applied a master equation expansion, showing that demographic noise leads to the spontaneous formation of species [30]. Traulsen *et al.* investigated evolutionary dynamics in unstructured populations using a stochastic differential equations approach [31]. Weitz *et al.* studied the co-evolution of bacteria and bacteriophage via mean-field and stochastic models [32]. While our investigation was partially motivated by these previous studies, our focus is different, namely on the influence of demographic variability on systems that exhibit the potential of evolutionary optimization.

We define our model in the following subsection 3.1. In subsection 3.2, we derive the associated mean-field equations and discuss their steady-state solutions. Finally, subsection 3.3 deals with the results of non-spatial as well as two-dimensional stochastic simulations and a comparison with the mean-field approximation.

3.1. Model Rules

We use the LV model as a basis for our study of individual variability, as explained already in section 1. In our model, particles of either species have an intrinsic property that describes their efficacy during predation reactions. More specifically, each particle carries a predation efficiency value η between zero and one. During a predation interaction between predator and prey particles with respective efficiency values η_A and η_B , we choose to determine the actual reaction rate from the arithmetic mean of these efficiencies:

$$\lambda = \frac{1}{2}(\eta_A + \eta_B). \tag{5}$$

Consequently, a predator particle with a high predation efficacy has a higher chance of consuming a prey and reproducing; it can be considered a good “hunter”. A prey particle with a low efficiency value is generally less likely to be consumed and can hence be labeled good at “evading”. Note that this efficiency value η differs from the fitness value that is derived from a certain genotype, which is often defined as the average number of offspring. Our net predation efficacy is a mesoscopic continuous stochastic

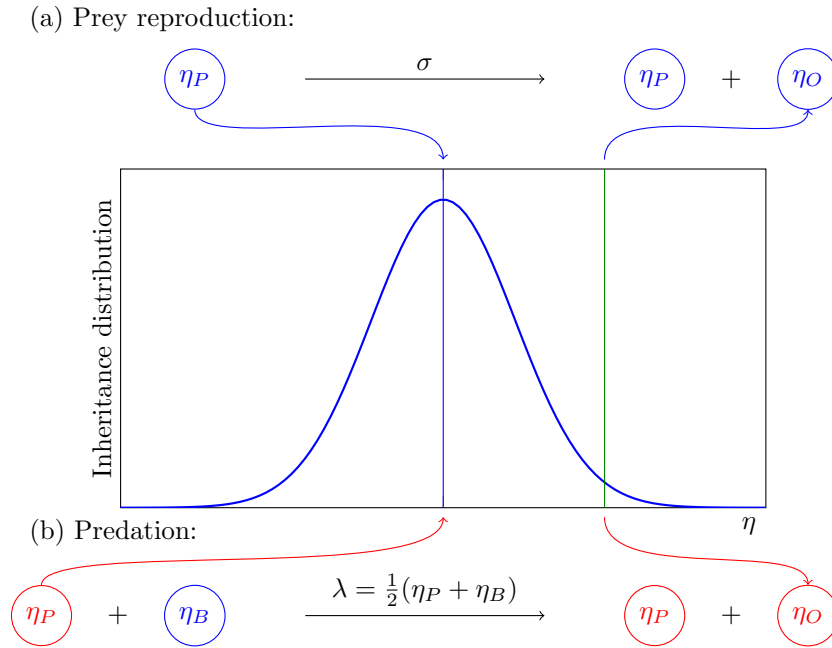


Figure 5. Inheritance model rules. (a) During prey reproduction, a parent particle spawns an offspring prey particle with a rate σ . The parent particle's predation efficiency value η_P is used as the mean of a Gaussian distribution, truncated to the interval between zero and one. The offspring's efficiency value η_O is then drawn from this inheritance distribution. (b) During predation, a predator particle consumes a prey particle with a rate λ , a function of the participating particles' predation efficiency values. A new offspring predator particle is created and its efficiency value η_O is determined via the same mechanism as is used in the case of prey reproduction.

variable that describes the combined effects of genetic makeup and strategy learning on the hunting or evasion capabilities of each individual.

We include inheritance and thus evolutionary dynamics in the predation efficiencies. We argued earlier that the predation efficiency value of an offspring particle is likely to be near the parent's value. Since the prime goal of this work is to investigate the influence of variability, we need to be able to control the average efficiency deviation between generations (i.e. the mutation probability). This suggests the use of a symmetric probability distribution that exhibits a maximum around the parent particle's efficiency value with a well-defined second moment.

Figure 5 shows how the predation efficiency is determined during the reproduction processes of prey and predator particles. The parent particle's efficiency value η_P is used as the mean value of a Gaussian distribution, truncated to the interval $[0, 1]$. The offspring's efficacy value η_O is then drawn from this inheritance distribution. The standard deviation of the Gaussian distribution (before truncation) w_P serves as the measure of variability in this scheme. It can also be viewed as the average severity of mutations from one generation to the next.

This variable inheritance of efficacies now allows for evolution of the hunting and evasion capabilities of the predator and prey populations. Selection processes due to

the predation reaction will optimize the steady-state population distributions of *both* species. There is however a notable asymmetry between the optimization mechanisms for the predator and prey populations, since the species interaction directly affects only the predator reproduction, whereas the prey population optimization happens through an indirect selection bias. We shall discuss this point further in section 3.3.

3.2. Doi-Peliti Formalism and Mean-Field Equations

In this subsection we systematically derive the mean-field equations for the LV model with inheritance of efficiencies. We start by writing down the model's master equation, which describes the time evolution of the probabilities of the system's microscopic states. We then switch to an equivalent Fock space formulation using particle creation and annihilation operators, which allows us to rewrite the master equation as an "imaginary-time Schrödinger equation". This yields a Liouville (or pseudo-Hamiltonian) time evolution operator. We write down the coherent-state 'action' in terms of the ladder operator eigenvalues and finally arrive at the mean-field equations for the predator and prey particle numbers. Their steady-state solutions can then be found numerically. Finally, we derive the exact solution in the case of a uniform inheritance distribution.

3.2.1. Master Equation. To construct the master equation of our LV-system with demographic variability and inheritance of a continuous efficiency variable, we need to find an equivalent system with a discrete set of states. To this end, we discretize the interval of possible predation efficiency values $0 \leq \eta \leq 1$ into N bins, with the bin midpoint values $\eta_i = (i + 1/2)/N$, $i = 0 \dots N - 1$. We then consider a predator or prey particle with an efficacy value in the range $\eta_i - 1/2 \leq \eta < \eta_i + 1/2$ to belong to the predator or prey subspecies i . The probability for the system to be in a state with a collection of $\{n_0, \dots, n_{N-1}\} \equiv \{n\}$ particles of subspecies of type A and $\{m_0, \dots, m_{N-1}\} \equiv \{m\}$ particles of subspecies of type B at time t is given by $P(\{n\}, \{m\}, t)$. In the following, the notation $\{n_i + 1\}$ indicates that there are $\{n_0, n_1, \dots, n_i + 1, \dots, n_{N-1}\}$ particles in the collection.

The probability that a particle with predation efficiency η_1 produces offspring with efficiency η_2 will be assigned using a reproduction probability function $f(\eta_1, \eta_2)$. We do not make any assumptions about the shape of this probability distribution other than that it be symmetric under exchange of its arguments, and that it be properly normalized with $\int_0^1 d\eta_1 f(\eta_1, \eta_2) = 1$. We use the discretized form $f_{ij} = f(\eta_i, \eta_j)$. The quantity $\lambda_{ij} = (\eta_i + \eta_j)/2$ finally provides the interaction rate of particles i and j .

Gathering the inflow and outflow terms of all reactions, we arrive at the master

equation of the LV system with demographic variability and evolutionary dynamics:

$$\begin{aligned}
 \frac{\partial P(\{n\}, \{m\}, t)}{\partial t} &= \mu \sum_i [(n_i + 1)P(\{n_i + 1\}, \{m\}, t) - n_i P(\{n\}, \{m\}, t)] \\
 &+ \sigma \sum_i \left[\sum_k (m_i - \delta_{ik}) f_{ik} P(\{n\}, \{m_k - 1\}, t) - m_i P(\{n\}, \{m\}, t) \right] \\
 &+ \sum_i \sum_j \lambda_{ij} \left[\sum_k (n_i - \delta_{ik}) (m_j + 1) P(\{n_k - 1\}, \{m_j + 1\}, t) - n_i m_j P(\{n\}, \{m\}, t) \right].
 \end{aligned} \tag{6}$$

As initial probability distribution $P(\{n\}, \{m\}, t_0)$, we choose independent Poisson distributions for both particle subspecies,

$$P(\{n\}, \{m\}, t_0) = \left(\prod_i \frac{\bar{n}_0^{n_i}}{n_i!} e^{-\bar{n}_0} \right) \left(\prod_j \frac{\bar{m}_0^{m_j}}{m_j!} e^{-\bar{m}_0} \right), \tag{7}$$

where the mean initial predator and prey species densities are denoted as \bar{n}_0 and \bar{m}_0 .

3.2.2. Equivalent Fock Space Formulation and the Time Evolution Operator. Because transitions between states of this system are uniquely identified by integer changes in the occupation numbers of the subspecies, we can introduce a general state $|\phi(t)\rangle$ through the linear combination

$$|\phi(t)\rangle = \sum_{\{n\}} P(\{n\}, \{m\}, t) |\{n\}, \{m\}\rangle, \tag{8}$$

of all possible basis states $|\{n\}, \{m\}\rangle = \prod_i |n_i\rangle |m_i\rangle$ for our system, weighted by the configurational probability of each state. By differentiating with respect to time, inserting the master equation (6) and shifting the summation over states, we obtain

$$\begin{aligned}
 \frac{\partial |\phi(t)\rangle}{\partial t} &= \sum_{\{n\}} \sum_{\{m\}} P(\{n\}, \{m\}, t) \left(\mu \sum_i n_i [|\{n_i - 1\}, \{m\}\rangle - |\{n\}, \{m\}\rangle] \right. \\
 &+ \sigma \sum_i m_i \left[\sum_k f_{ik} |\{n\}, \{m_k - 1\}\rangle - |\{n\}, \{m\}\rangle \right] \\
 &\left. + \sum_i \sum_j \lambda_{ij} n_i m_j \left[\sum_k f_{ik} |\{n_k + 1\}, \{m_j - 1\}\rangle - |\{n\}, \{m\}\rangle \right] \right).
 \end{aligned}$$

Next we introduce raising and lowering operators in complete analogy to a quantum-mechanical harmonic oscillator or bosonic Fock states. We need two sets of operators, a_i, a_i^\dagger and b_i, b_i^\dagger for species A and B, respectively. The operators act on the states in the following manner:

$$\begin{aligned}
 a_i^\dagger |\{n\}, \{m\}\rangle &= |\{n_i + 1\}, \{m\}\rangle, \\
 a_i |\{n\}, \{m\}\rangle &= n_i |\{n_i - 1\}, \{m\}\rangle, \\
 b_i^\dagger |\{n\}, \{m\}\rangle &= |\{n\}, \{m_i + 1\}\rangle, \\
 b_i |\{n\}, \{m\}\rangle &= m_i |\{n\}, \{m_i - 1\}\rangle, \\
 [a_i, a_j^\dagger] &= \delta_{ij} = [b_i, b_j^\dagger],
 \end{aligned} \tag{9}$$

guaranteeing that the occupation number operators $a_i^\dagger a_i$ and $b_i^\dagger b_i$ have integer eigenvalues. This procedure finally yields the time evolution or Liouville operator of our system

$$H = \sum_i \left[\mu(a_i^\dagger - 1)a_i + \sigma \left(1 - \sum_k f_{ik} b_k^\dagger \right) b_i^\dagger b_i + \sum_j \lambda_{ij} \left(b_j^\dagger - \sum_k f_{ik} a_k^\dagger \right) a_i^\dagger a_i b_j \right]. \quad (10)$$

Note that one may obtain this result from the reaction Liouville operator of the standard LV system [17] by replacing $1 - b_i^\dagger \rightarrow 1 - \sum_k f_{ik} b_k^\dagger$ in the prey reproduction term, as well as $b_j^\dagger - a_j^\dagger \rightarrow b_j^\dagger - \sum_k f_{jk} a_k^\dagger$ and $\lambda \rightarrow \sum_j \lambda_{ij}$ (with the appropriate change in the indices) in the predator reproduction term, as one would expect.

3.2.3. Coherent-State 'Action' and Mean-Field Equations. To calculate observable averages $\langle O(t) \rangle = \sum_{\{n\}} \sum_{\{m\}} O(\{n\}, \{m\}) P(\{n\}, \{m\}, t)$ one needs to introduce a projection state $\langle P| = \langle 0| \prod_i e^{a_i} e^{b_i}$ with $\langle P|0 \rangle = 1$ and $\langle P|a_j^\dagger = \langle P| = \langle P|b_j^\dagger$ due to $[e^{a_i}, a_j^\dagger] = e^{a_i} \delta_{ij}$ [17]. We can then write observable averages as

$$\langle O(t) \rangle = \langle P| O(\{n\}, \{m\}) |\phi(t) \rangle. \quad (11)$$

Due to probability conservation $1 = \langle P|\phi(t) \rangle = \langle P|e^{-Ht}|\phi(0) \rangle$ must hold and hence, $\langle P|H = 0$ since $\langle P|\phi(0) \rangle = 1$, and thus $H(a_i, b_i, a_i^\dagger \rightarrow 1, b_i^\dagger \rightarrow 1) = 0$.

Next, we introduce ladder operator coherent states, familiar from many-particle quantum mechanics. The right eigenstates of the predator annihilation operator a_i with eigenvalue α_i are $|\alpha_i \rangle = \exp(-|\alpha_i|^2/2 + \alpha_i a_i^\dagger) |0\rangle$, which can be easily checked by inserting into $a_i |\alpha_i \rangle = \alpha_i |\alpha_i \rangle$. These states are overcomplete in the sense that $\int \prod_i d\alpha_i^* d\alpha_i |\alpha_i \rangle \langle \alpha_i| = \pi$. An analogous set of right eigenstates can be introduced for the prey annihilation operator $\beta_i |\beta_i \rangle = \beta_i |\beta_i \rangle$. By repeatedly inserting the overcompleteness relation of both sets of states into the time-dependent observable (11), and following the analysis done in reference [17] (described more generally in reference [33]), we arrive at a path integral expression for calculating averages:

$$\langle O(t) \rangle = N^{-1} \int \prod_i d\alpha_i^* d\alpha_i d\beta_i^* d\beta_i O(\{\alpha_i\}, \{\beta_i\}) \exp(-S[\{\alpha_i^*\}, \{\alpha_i\}, \{\beta_i^*\}, \{\beta_i\}, t]). \quad (12)$$

The normalization is determined by calculating the average of the identity operator $N = \int \prod_i d\alpha_i^* d\alpha_i d\beta_i^* d\beta_i e^{-S}$. The coherent-state path integral 'action' (the exponential weight in the path integral) then becomes

$$\begin{aligned} S[\{\alpha_i^*\}, \{\alpha_i\}, \{\beta_i^*\}, \{\beta_i\}, t] = & \sum_i \left(-\alpha_i(t) - \beta_i(t) - \bar{n}_0 \alpha_i^*(0) - \bar{m}_0 \beta_i^*(0) \right. \\ & + \int_0^t dt' \left[\alpha_i^* \frac{\partial \alpha_i}{\partial t'} + \beta_i^* \frac{\partial \beta_i}{\partial t'} + \mu(\alpha_i^* - 1)\alpha_i + \sigma \left(1 - \sum_k f_{ik} \beta_k^* \right) \beta_i^* \beta_i \right. \\ & \left. \left. + \sum_j \lambda_{ij} \left(\beta_j^* - \sum_k f_{ik} \alpha_k^* \right) \alpha_i^* \alpha_i \beta_j \right] \right). \end{aligned} \quad (13)$$

The terms in which the fields explicitly depend on the final time stem from the projection state and can be safely ignored for averages and correlation functions that do not explicitly depend on these times, as is the case here. The variables \bar{n}_0 and \bar{m}_0 respectively represent the average initial number of prey and predator particles in each subspecies, and originate in the initial Poisson distribution (7).

The classical equations of motion for the fields α_i^* , α_i , β_i^* and β_i are determined by using the steepest-descent method, i.e. the minimum of S with respect to the fields. Hence we set the variation of S to zero:

$$\frac{\delta S}{\delta \alpha_i} = 0 = -\frac{\partial \alpha_i^*}{\partial t} + \mu(\alpha_i^* - 1) + \sum_j \lambda_{ij} \left(\beta_j^* - \sum_k f_{ik} \alpha_k^* \right) \alpha_i^* \beta_j, \quad (14)$$

$$\frac{\delta S}{\delta \beta_i} = 0 = -\frac{\partial \beta_i^*}{\partial t} + \sigma \left(1 - \sum_k f_{ik} \beta_k^* \right) \beta_i^* + \sum_j \lambda_{lj} \left(\beta_i^* - \sum_k f_{jk} \alpha_k^* \right) \alpha_j^* \alpha_j, \quad (15)$$

$$\frac{\delta S}{\delta \alpha_i^*} = 0 = \frac{\partial \alpha_i}{\partial t} + \mu \alpha_i + \sum_j \lambda_{ij} \left(\beta_j^* - \sum_k f_{ik} \alpha_k^* \right) \alpha_i \beta_j - \sum_{kj} \lambda_{ij} f_{ki} \alpha_k^* \alpha_k \beta_j, \quad (16)$$

$$\begin{aligned} \frac{\delta S}{\delta \beta_i^*} = 0 = & \frac{\partial \beta_i}{\partial t} + \sigma \left(1 - \sum_k f_{ik} \beta_k^* \right) \beta_i - \sigma \sum_k f_{ki} \beta_k^* \beta_k + \sum_j \lambda_{ji} \alpha_j^* \alpha_j \beta_i \\ & + \sum_j \lambda_{ji} \left(\beta_i^* - \sum_k f_{ik} \alpha_k^* \right) \alpha_i^* \alpha_i. \end{aligned} \quad (17)$$

Equations (14) and (15) are readily solved by $\alpha_i^* = 1 = \beta_i^*$, a consequence of probability conservation. Equations (16) and (17) then yield the classical equations of motion for the fields α_i and β_i . Since the predator and prey subspecies counts are $a_i(t) = \langle P | n_i | \phi(t) \rangle = \alpha_i(t)$ and $b_i(t) = \langle P | m_i | \phi(t) \rangle = \beta_i(t)$, we arrive at the coupled mean-field equations for our system:

$$\frac{\partial a_i(t)}{\partial t} = -\mu a_i(t) + \sum_{jk} \lambda_{kj} f_{ki} a_k(t) b_j(t), \quad (18)$$

$$\frac{\partial b_i(t)}{\partial t} = \sigma \sum_k f_{ki} b_k(t) - \sum_j \lambda_{ji} a_j(t) b_i(t). \quad (19)$$

These equations look very similar to the standard LV rate equations (2). In fact, setting $f_{ij} = \delta_{ij}$ and $\lambda_{ij} = \lambda \delta_{ij}$ yields the standard LV mean-field rate equations for each subspecies i .

3.2.4. Steady-State Solutions. Steady-state solutions of the mean-field equations (18) and (19) are determined by setting the time derivatives to zero: $\partial a_i(t)/\partial t = 0 = \partial b_i(t)/\partial t$. Therefore, the steady-state particle counts can always be found by numerically solving the coupled implicit equations

$$\mu a_i = \sum_{jk} \lambda_{kj} f_{ki} a_k b_j, \quad (20)$$

$$\sigma \sum_k f_{ki} b_k = \sum_j \lambda_{ji} a_j b_i, \quad (21)$$

using a self-consistent, iterative approach.

In the special case of a uniform inheritance distribution $f_{ij} = 1/N$, the steady-state counts can be found exactly. In this situation, there are no correlations between the parent and offspring particle efficiencies, and the right-hand side of equations (20) becomes independent of the index i . Consequently, the number of predators in bin i is constant and independent of i , whence $a_i = \text{const} = A$. Equation (21) can be rewritten as

$$\frac{b_i}{\sum_k b_k} = \frac{\sigma}{AN} \frac{2N}{\sum_j (i+j+1)}. \quad (22)$$

Summing both sides over i and using $\sum_j 1 = N$ and $\sum_j j = N(N-1)/2$ gives

$$\frac{AN}{2\sigma} = \sum_i \frac{1}{i + \frac{N+1}{2}}.$$

Using a difference equation involving the digamma function $\psi(x+N) - \psi(x) = \sum_i \frac{1}{i+x}$ yields

$$\frac{AN}{2\sigma} = \psi\left(\frac{3N+1}{2}\right) - \psi\left(\frac{N+1}{2}\right).$$

In order to find a useful, approximate value of the constant A , we rewrite this expression in the form

$$\frac{AN}{2\sigma} = \ln\left(\frac{3N+1}{N+1}\right) + \frac{1}{3N+1} - \frac{1}{N+1} - \sum_{n=1}^{\infty} \frac{2^{2n-1} B_{2n}}{n} \left[\frac{1}{(3N+1)^{2n}} - \frac{1}{(N+1)^{2n}} \right],$$

where we have used the asymptotic series expansion of the digamma function

$$\psi(x) = \ln x + \frac{1}{2x} - \sum_{n=1}^{\infty} \frac{B_{2n}}{2nx^{2n}}$$

(B_k is the k -th Bernoulli number). Hence, in the limit of large N , the constant simplifies to

$$\lim_{N \rightarrow \infty} \frac{AN}{2\sigma} = \ln 3.$$

Defining the subspecies densities as $\rho_{a,i} = a_i / \sum_j a_j$ and $\rho_{b,i} = b_i / \sum_j b_j$, and using equation (22), as well as the definition of the efficiency bins $\eta_i = (i+1/2)/N$, we finally arrive at

$$\rho_a = \frac{1}{N}, \quad \rho_{b,i} = \frac{2}{N \ln 3} \frac{1}{1+2\eta_i}, \quad (23)$$

which is valid in the limit of large N . Hence, the predator density becomes constant and independent of the subspecies index i . The prey density exhibits a selection bias towards low values of the efficiency η .

3.3. Population Distributions from Simulations

We are now ready to perform Monte Carlo simulations of our system. Our main goal in this section is to extract the predator and prey population distributions as a function of the particle efficiencies. To this end, we introduce efficiency bins $\eta_i = (i + 1/2)/N$, $i = 0, \dots, N - 1$ in complete analogy to the derivation of the master equation in section 3.2.1. We then count the number of particles a_i and b_i in the interval $[\eta_i - 1/(2N), \eta_i + 1/(2N))$ and calculate the densities $\rho_{A,i} = a_i / \sum_j a_j$ and $\rho_{B,i} = b_i / \sum_j b_j$. The resulting histograms approximate the population distributions as a function of the efficacies.

Our simulations start by assigning all particles an initial predation efficiency of $\eta_{A/B} = 0.5$. Hence the population distributions for $t = 0$ exhibit a sharp peak at $\eta = 0.5$ and are zero everywhere else. This choice is mainly due to computational convenience, since the final steady-state population distributions do not depend on the initial state of the system. We checked this statement by varying the initial distribution of particles in efficiency space. There of course exist initial conditions in which the probability of one or both of the species to go extinct is rather high. Since we are interested only in steady states that exhibit species coexistence, we exclude those initial conditions from our considerations. The reproduction and mortality rates are both set to $\sigma = \mu = 0.5$.

Spatial as well as intrinsic temporal correlations in stochastic simulations renormalize the results relative to the mean-field predictions given by equations (20) and (21). A comparison of our data for zero-dimensional, non-spatial systems with the results taken in spatially extended systems allows us to disentangle the effects of purely temporal and spatial correlations.

We let the system and thus the population distributions evolve over time, via random sequential Monte Carlo updates. One Monte Carlo step is complete when, on average, each particle in the system has been selected once. The predator and prey populations optimize their predation efficiency over many generations. In each simulation run, we wait until the population distributions have reached their (quasi-) steady-state shapes. Predators benefit from a higher efficacy value, because their average interaction and thus reproduction rate is enhanced. Hence, a predator with a high η is more likely to have more offspring, compared to a low- η predator particle, which in turn inherits this high η value. This yields an overall optimization of the predator population towards high efficacies. Prey particles on the other hand benefit from low predation efficiency values, because their average lifetime is longer than for individuals with high η . Hence a reduced η value yields a larger number of prey offspring particles and, accordingly, the same optimization as for the predator population occurs, only towards low η values. This dynamic, evolutionary optimization finally leads to a steady-state efficacy distribution among the individual particles when the distance of the population maxima from the efficiency edges $\eta = 0, 1$ is balanced by the finite width of the inheritance distribution.

Figure 6 displays the population distributions as functions of the efficiency η for

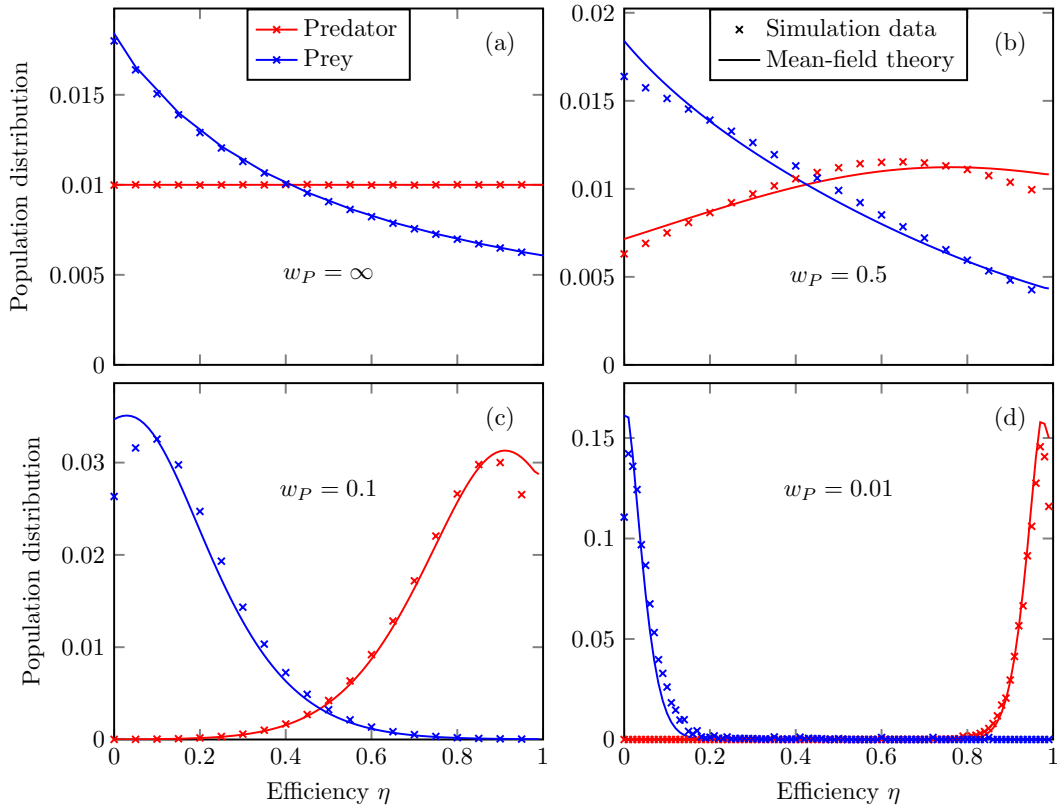


Figure 6. Population distributions for various values of the inheritance distribution width w_P . The red and blue curves respectively indicate the predator and prey populations as functions of the efficiency. Curves with \times markers stem from zero-dimensional (well-mixed) simulations, while the solid lines show the mean-field predictions. (a) Population distribution for a uniform inheritance distribution with $w_P = \infty$. The prey population displays an inherent selection bias towards low η , while the predator population is flat. The mean-field prediction (23) exactly agrees with the simulation data. (b) Population distribution for a broad inheritance distribution with $w_P = 0.5$. The inherent selection bias of the prey population is still visible, but overlaid with the dynamic optimization towards low η . The predator population optimizes towards higher η and shows a maximum around $\eta \approx 0.65$. Our numerical mean-field model solution is in qualitative agreement. (c) Population distributions for a narrow inheritance distribution with $w_P = 0.1$. Both predator and prey populations are optimized towards high and low values of η with maxima at $\eta \approx 0.9$ and $\eta \approx 0.1$, respectively. Mean-field theory over-estimates the optimization effects and places the population maxima slightly closer towards the efficiency extrema. (d) Population distribution data for a sharply peaked inheritance distribution with $w_P = 0.01$. The maxima move even closer to the edges of the efficiency range. The results represent an ensemble average over 1000 realizations.

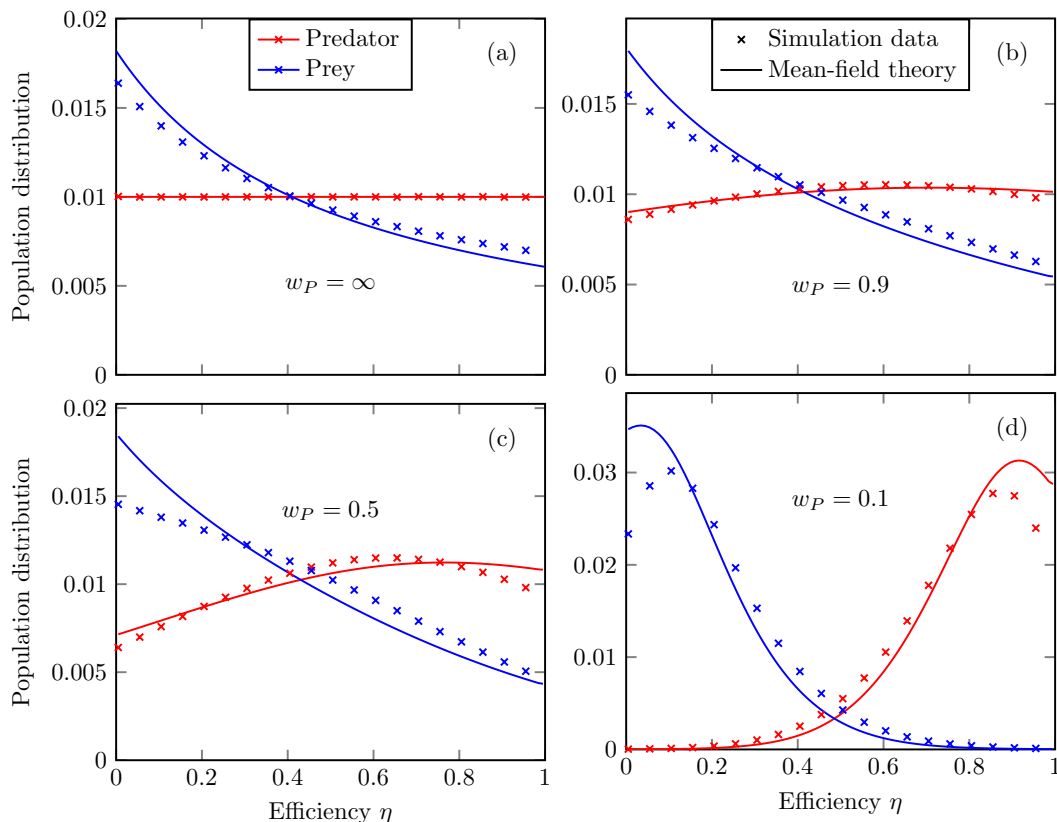


Figure 7. Population distributions for various values of the inheritance distribution width w_P from two-dimensional lattice simulations. The red and blue curves respectively indicate the predator and prey populations as a function of the efficiency. Curves with \times markers stem from simulations, while the solid lines show the results from mean-field theory. (a) Population distribution for a uniform inheritance distribution with $w_P = \infty$. The mean-field prediction for the prey population (23) ignores spatial correlations and thus over-estimates the prey selection bias in this case. (b-d) Population distributions for broader inheritance distributions with $w_P = 0.9, 0.5, 0.1$, respectively. The mean-field prediction deviates more strongly from the simulation data than in the case of well-mixed zero-dimensional simulations. The results represent an ensemble average over 10000 realizations.

various values of the inheritance distribution width w_P . The special case of an infinite width $w_P = \infty$ is shown in figure 6(a). In this situation, no correlation exists between the efficacies of a parent and its offspring, and the efficiency assignment during reproduction is completely random. Consequently, the predator population distribution is flat and independent of η , as predicted by our mean-field theory result (23). The prey population distribution shows an inherent selection bias towards low values of η . A low efficiency for a prey particle means that it is more likely to live longer than another individual with higher efficiency, according to our formula for the predation rate (5). Hence, at any given time when the system is in the (quasi-) steady state, there needs to be a higher number of prey particles in the low-efficiency bins than in the higher ones. This result and the simulation data agree perfectly with our mean-field theory result (23) as well,

without any fit parameters.

For non-uniform inheritance distribution, evolutionary optimization of the predator and prey populations takes place. Figure 6(b) shows the population distribution for $w_P = 0.5$. In this case, the effects of the inherent prey selection bias are still apparent and no clear prey population maximum is visible. The predator population exhibits a maximum at $\eta \approx 0.65$ due to the balancing of dynamic optimization and the finite width of the inheritance distribution. The numerical, self-consistent solution of our mean-field equations agrees qualitatively with the simulation data, but over-estimates the effects of optimization. At an even smaller inheritance distribution width of $w_P = 0.1$, the predator and prey population distributions, displayed in figure 6(c), form clear maxima at high and low values of η , respectively. Again, the numerical mean-field predictions over-estimate optimization effects and place the population maxima nearer to the efficacy edges $\eta = 0, 1$. A sharply peaked inheritance distribution with $w_P = 0.01$ yields population maxima even closer to the edges of the efficiency range, as shown in 6(d).

Spatially extended, two-dimensional lattice simulations yield quantitatively slightly different predator and prey population distributions. Emerging spatial correlations influence the results as shown in figure 7. Since mean-field theory ignores spatial correlations, our solution already over-estimates the prey selection bias in the two-dimensional model, but is still qualitatively correct. A similar trend is noticeable for finite values of the inheritance distribution width w_P . Note that spatial correlations lead to less sharply peaked population distributions than in the case of non-spatial simulations. Hence we may conclude that intrinsic, temporal correlations and spatial correlations both induce a smoothening of sharp features in the population distributions.

4. Spatial vs. Demographic Variability

We now introduce *quenched spatial* randomness in addition to demographic variability, which we discussed in the last section. We wish to clarify the relative importance of both types of variability in the interaction rate on the evolutionary optimization dynamics of our two-species LV predator-prey system. To this end, we need to introduce a new control parameter ζ that allows us to tune the relative influence of environmental and demographic randomness.

We model environmental variability by introducing a new lattice site-dependent quenched random variable, the spatial efficiency η_S , similar as in our discussion for purely environmental variability in section 2. Before the start of a new simulation run, the environment is generated by assigning a value to this variable on each lattice site, drawn from a Gaussian distribution of width w_S , centered around a value of $\overline{\eta_S} = 0.5$ and truncated to the interval $[0, 1]$. The distribution width w_S is a model parameter and provides a measure of spatial variability similar to the mutation probability discussed previously. The rate at which an interaction between two specific predator and prey

individuals occurs on a given lattice site is now a function of η_S , η_A , and η_B :

$$\lambda = \zeta\eta_S + (1 - \zeta)\frac{\eta_A + \eta_B}{2}. \quad (24)$$

The spatial influence parameter ζ varies between 0 and 1 and smoothly tunes between purely spatial and individual variabilities.

Here, the system consists of a square lattice with 128×128 sites and periodic boundary conditions. We did not discern any finite-size effects already at this lattice size. Predator and prey particles perform unbiased random walks on this lattice, with a per-step probability of one. Thus all rates in the system are to be understood as measured in units of the diffusivity D . The predation, reproduction, and death reactions occur on-site, without per-site particle number restrictions. The predator extinction transition, present in systems with site restrictions, is thus absent here [34, 18, 19]. The prey reproduction and predator death rates are fixed and both set to $\sigma = \mu = 0.5$. Predator and prey particles are initially distributed at random throughout the lattice, with average densities $\rho_A = \rho_B = 1$. Similar to the zero-dimensional case discussed in section 3.3, the initial individual efficiencies of our particles are set to $\eta_A = \eta_B = 0.5$, but the final steady-state properties turn out not to depend on these initial values. The simulation proceeds via random sequential Monte Carlo updates, where during each iteration a random particle is selected and moved to a randomly chosen neighboring site. The particle is then allowed to perform a reproduction reaction if it is a prey, or a predation and subsequent mortality reaction if it is a predator, with the assigned rates. During a predation reaction, the rate is calculated according to equation (24). Again, one Monte Carlo step (MCS) is complete when, on average, each particle in the system has been selected once.

4.1. Steady-State Particle Density

We measure the steady-state particle density as a function of the individual variability w_P , the spatial variability w_S and the spatial importance factor ζ . During each simulation realization we let the system run for 700 MCS to reach the stationary state and subsequently average the predator and prey particle densities over an additional 300 MCS. The resulting data is then averaged over an ensemble of 10000 realizations per parameter combination. The investigated ranges for the parameters where $w_P, w_S \in [0, 0.9]$ and $\zeta \in [0, 1]$. Figure 8(a) shows the normalized predator population change as a function of variability for purely individual ($w_P = w, w_S = 0$), purely spatial ($w_P = 0, w_S = w$), and equal ($w_P = w_S = w$) variabilities, with $\zeta = 0.3$ (the location of the minimum discussed below). In the case of purely individual variability we observe a small population increase of $\approx 1.5\%$. Purely spatial variability leads to a slightly larger increase of $\approx 4\%$, and the mixed case yields the largest increase of just below 6%. This hierarchy holds true for all values of ζ . Figure 8(b) displays the population increase for the mixed case, as a function of ζ for different values of w . The purely individual ($\zeta = 0$) and purely spatial ($\zeta = 1$) efficiency cases yield local maxima in the population increase,

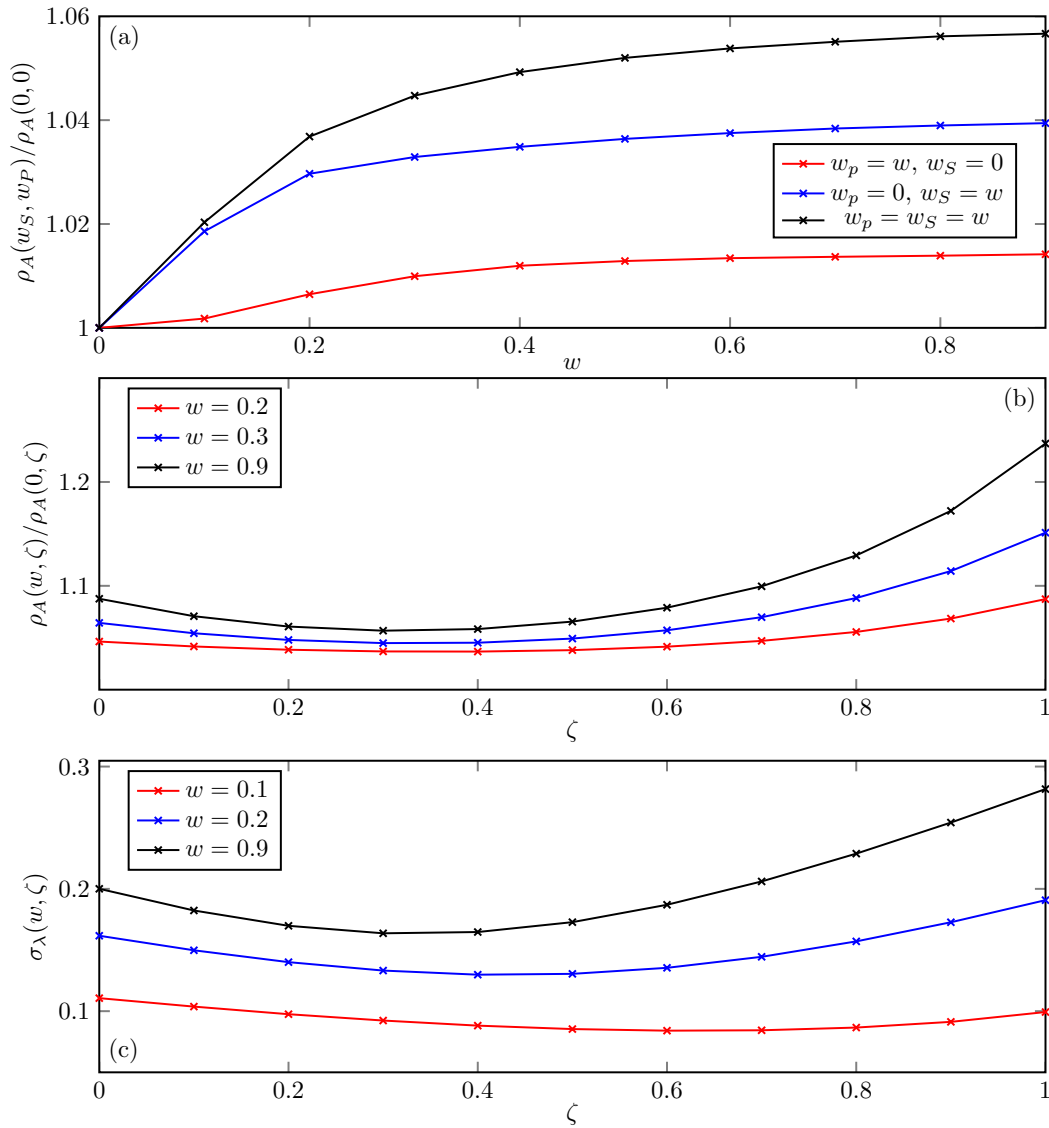


Figure 8. The (quasi-)steady state predator density as a function of spatial and individual variability, as well as spatial influence. (a) The normalized (quasi-)steady state predator density ρ_A as a function of variability w for $\zeta = 0.3$ for the cases of purely individual ($w_P = w, w_S = 0$), purely spatial ($w_P = 0, w_S = w$), and equal variabilities ($w_P = w_S = w$). (b) The normalized predator density as a function of ζ for equal variabilities $w_P = w_S = w$ for $w = 0.2, w = 0.3$, and $w = 0.9$. For all values of w , a remarkable minimum is observed. (c) The standard deviation of the predation rate σ_λ for the same cases as in (b), calculated via error propagation from the spatial and individual predation efficiency distributions also shows the minimum.

whence we observe a remarkable minimum for all values of w for intermediate values of ζ . Purely spatial efficiency leads to the highest observed population density, an increase of just under 25% over the non-disordered system. Purely individual rates yield a moderate increase of 8%. Figure 8(c) shows the standard deviation for the predation rates λ , $\sigma_\lambda = \sqrt{\zeta^2\sigma_S^2 + (1-\zeta)^2(\sigma_A^2 + \sigma_B^2)}/2$, as a function of ζ and w . Since the spatial and individual predation efficiency values are truncated to the interval $[0, 1]$, the standard deviation of their actual distribution is different from the variability measure w , and therefore needs to be calculated from simulation data on the population distributions in efficiency space, and the distribution of spatial efficiency values on the lattice. The standard deviation follows a similar shape as compared to the population density shown in figure 8(b); in particular the two local maxima at $\zeta = 0$ and $\zeta = 1$, as well as the minimum in between are reflected here.

Our data clearly demonstrate that the population density increase is primarily a monotonic function of the overall variance of the predation rate λ . The two types of variability do not simply contribute additively or multiplicatively, since the evolutionary dynamics in the demographic variability renders the relationship more complex. The disproportionate increase of the population densities for $\zeta = 1$ over $\zeta = 0$, compared to the standard deviation, also leads us to conclude that the effect of spatial variability is markedly more pronounced as compared to demographic variability.

In section 3.2.4, we observed that the evolutionary dynamics inherent to our model of demographic variability leads to optimization of the population distributions in efficiency space for *low* values of the variability w_P . This becomes progressively weaker for higher w_P . Here, we observe a population increase for *high* variability, and a very weak to non-existent increase for lower w . Hence, we argue that the optimization of population distributions in efficiency space is essentially *neutral* towards the overall species densities (at least in the context of our model). The net benefit of optimizing the predator population towards high values of the individual efficiency and the prey populations towards low efficacies is almost zero. The optimization is however crucial for the survival of either species during their competitive co-evolution, reminiscent of an arm's race scenario.

4.2. Correlation Lengths and Decay Time

We calculate correlation lengths by evaluating the spatial density correlation functions

$$C_{ij}(x) = \langle \rho_i(0)\rho_j(\vec{x}) \rangle - \langle \rho_i \rangle \langle \rho_j \rangle, \quad (25)$$

where the indices i and j stand for either species A or B , and the angular brackets indicate an average over all lattice sites as well as an ensemble average over 10000 realizations. The single-species auto-correlation functions C_{AA} and C_{BB} display a simple exponential decay $C_{ii}(x) \propto \exp(-x/l_{ii})$, from which we extract the correlation length via a numerical derivative $l_{ii} = -d \ln C_{ii}(x)/dx$. The species cross-correlation function C_{AB} is negative for small x , has a positive maximum at intermediate x , and

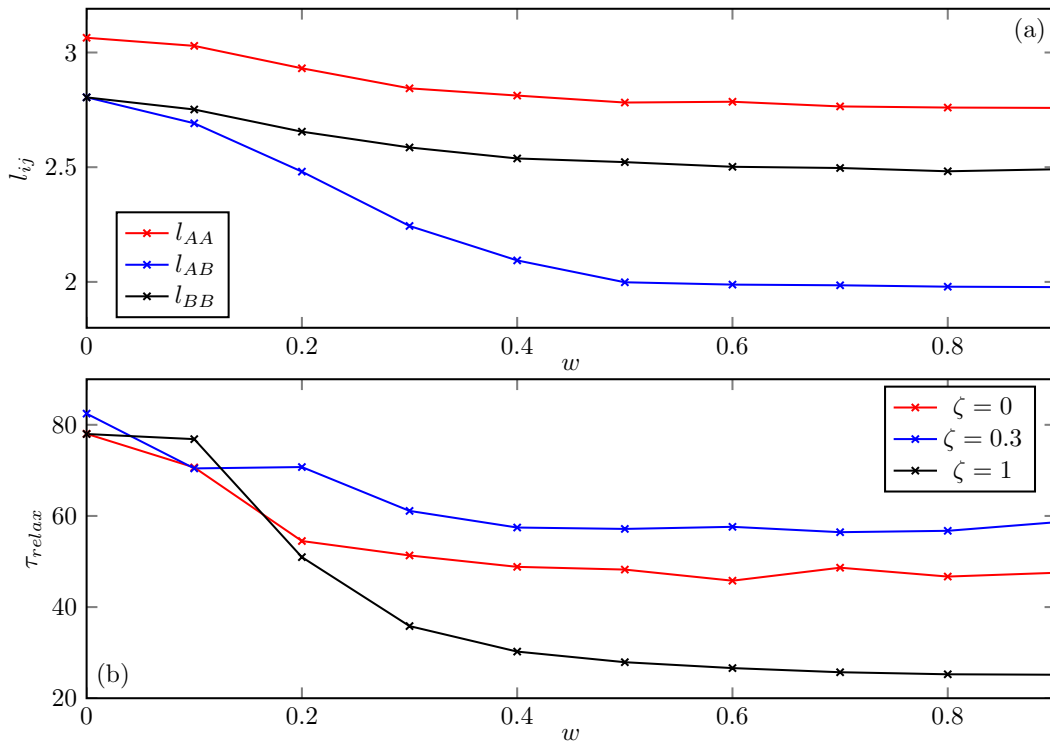


Figure 9. Correlation lengths and relaxation time as a function of variability. (a) The autocorrelation lengths l_{AA} and l_{BB} as well as the cross-correlation length l_{AB} from the species autocorrelation functions for $\zeta = 0.6$. (b) The predator density relaxation time τ_{relax} toward the quasi-stationary state for different values of ζ .

decays to zero for large x . We numerically extract the position of this maximum, the typical distance between predator and prey particles l_{AB} . Figure 9(a) shows the correlation lengths l_{AA} and l_{BB} , as well as the typical distance l_{AB} as a function of ζ for $w = 0.9$. These characteristic lengths decrease with increasing variability, which indicates that the particles in the system are packed more densely. In reference [1] we argued that environmental variability leads to the formation of safe havens for prey, where the predation rate is very small and prey can proliferate. The predator particles then feed off the prey particles that diffuse away from the activity patches, yielding the observed compression of the system. In reference [2] we observed that a similar mechanism occurs in the presence of demographic variability, but here these activity patches are due to highly optimized low-efficiency prey particles proliferating and thus ephemeral. Consequently the effect of demographic variability on the steady-state densities is smaller than the influence of environmental variability.

We additionally investigated the relaxation properties of the LV system in the presence of both types of variability. To this end, we Fourier-transformed time traces of the predator density [for an example see figure 2(a)] and fitted a Gaussian function to the resulting peak. The peak width is then inversely proportional to the relaxation time $\tau_{relax}(w, \zeta)$. Figure 9(b) shows a consistent decrease in the relaxation time of up to a factor of 0.3 due to the presence of variability.

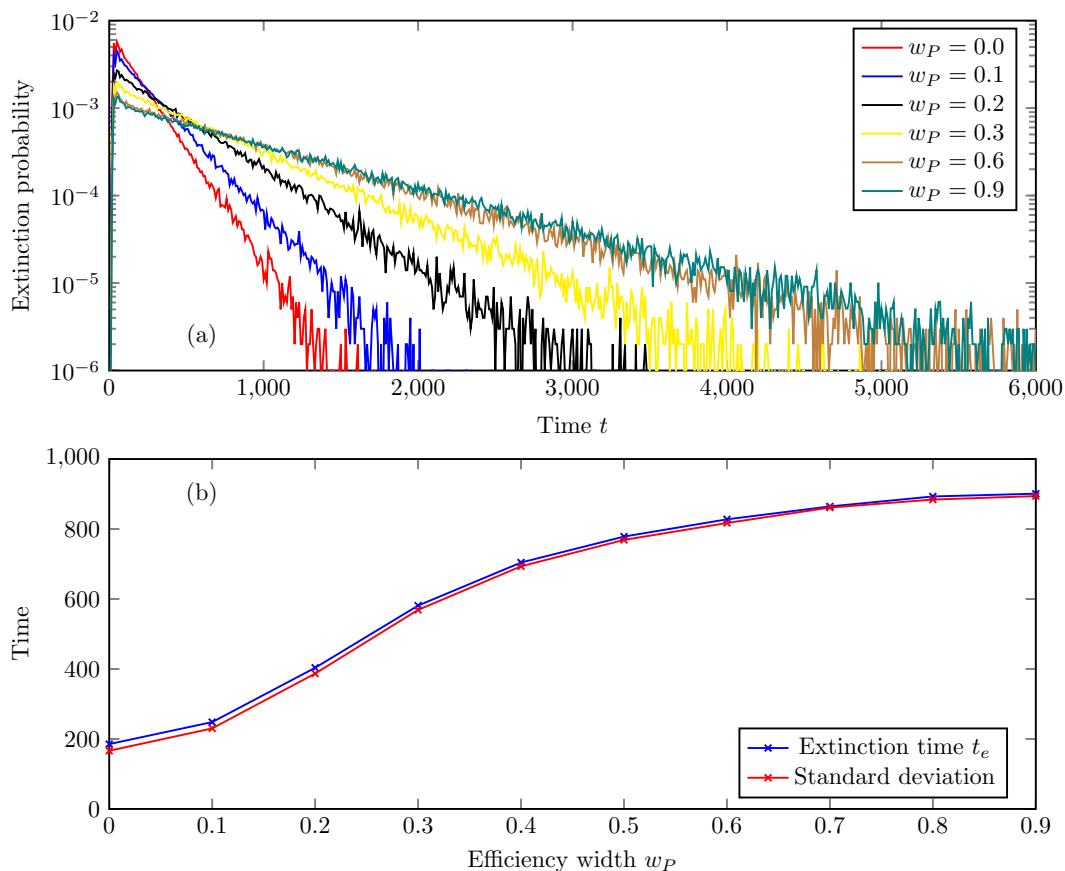


Figure 10. Extinction time probability and mean extinction time in a small system of 10×10 lattice sites as functions of individual variability w_P . Only individual efficiencies are considered here, $\zeta = 0$. (a) Normalized extinction event histograms as functions of time for different widths of the efficiency inheritance distribution w_P . In the case of zero variability $w_P = 0$, extinction events are mostly confined to the time regime $t < 1000$. For higher values of w_P the tail of the extinction event distribution moves to longer times and becomes increasingly broader. (b) The mean extinction time t_e (blue) shows a more than four-fold increase as a function of the variability w_P . Its standard deviation (red) has approximately the same value as t_e , which is consistent with an exponential extinction distribution in the long-time limit.

4.3. Extinction Statistics

In finite stochastic systems with an absorbing state (here, predator extinction), fluctuations will eventually drive the system into the absorbing state, as discussed in section 1.3 and references [22, 18]. This can be exploited to gain information about the stability of our model against the extinction of either species as a function of the model parameters. To this end, we simulated small systems, with a lattice size of 10×10 sites, until the number of particles of either the prey or the predator species reaches zero, and collected the simulation time up to this event into extinction time histograms. The normalized extinction event count then corresponds to the extinction event probability $P_e(t)$.

Figure 10(a) depicts the extinction data for selected values of the variability w_P . The histograms show that the extinction probabilities are consistent with an exponential distribution in the long-time limit [35, 36]. For increasing variability, the extinction event distributions become increasingly broader. Figure 10(b) shows the mean extinction time $t_e = \sum_{t=0}^{\infty} tP_e(t)$ and its standard deviation $\sigma_e = \sqrt{\sum_{t=0}^{\infty} (t - t_e)^2 P_e(t)}$ as a function of the inheritance distribution width w_P . The mean extinction time is enhanced by a factor of up to ≈ 4.5 due to individual variability. This, together with the increase in σ_e , indicates that a higher number of realizations of our small system survive for longer times. Hence, we conclude that individual variability renders our model more robust against extinction.

5. Conclusions

In this paper, we have studied and discussed a particular variant of the LV model in which we introduced two different kinds of variability into the predator-prey interaction rate. In an earlier study, we investigated the effects of purely spatial variability of the predation rate and found a marked increase in the steady-state population densities of both species; see section 2 and reference [1].

Here, we introduced demographic variability together with evolutionary dynamics, in which during a reproduction step, the offspring particle inherits an efficiency close to its parent's value. The resulting steady-state optimization, discussed in section 3.3, yields predator and prey populations that are located at high and low values of the efficiency, respectively. We were able to find good agreement of the simulation data with our effective subspecies mean-field model derived in section 3.2. Our results show that this population level optimization has negligible effects on the overall population densities, but is necessary for species survival.

In section 4, we discussed our results for a spatially extended system in which both types of variability, environmental and demographic, are present. We found that demographic variability leads to an increase of the steady-state densities of both species, similar to our previous results for purely spatial randomness but smaller in magnitude. By investigating correlation functions, we demonstrated that the system becomes denser, supporting our argument that variability causes more localized activity patches, where prey proliferate and predators feed off prey that diffuse away from these patches. Additionally, extinction event histograms show that enhanced variability renders the system more stable against the extinction of either species.

This extensive numerical Monte Carlo simulation study of environmental and demographic variability highlights the importance of randomness on the dynamics of ecological models. While a simple two-species predator-prey system has limited predictive power for real ecological neighborhoods, these results still emphasize the need to investigate variability in more complex models, such as food webs.

We gratefully acknowledge inspiring discussions with G. Daquila, E. Frey, J. Phillips, T. Platini, M. Pleimling, B. Schmittmann, and R.K.P. Zia.

References

- [1] Dobramysl U and Täuber U C. Spatial Variability Enhances Species Fitness in Stochastic Predator-Prey Interactions, 2008 *Phys. Rev. Lett.* **101** 258102.
- [2] Dobramysl U and Täuber U C. Environmental Versus Demographic Variability in Two-Species Predator-Prey Models, 2013 *Phys. Rev. Lett.* **110** 048105.
- [3] May R. *Stability and complexity in model ecosystems*. Princeton University Press, Princeton, NJ, 1973.
- [4] Smith J. *Models in ecology*. Cambridge University Press, Cambridge, 1974.
- [5] Murray J D. *Mathematical Biology*, volume I and II. Springer, New York, 3rd edition, 2002.
- [6] Hofbauer J and Sigmund K. *Evolutionary Games and Population Dynamics*. Cambridge University Press, Cambridge, 1998.
- [7] He Q, Mobilia M, and Täuber U C. Spatial rock-paper-scissors models with inhomogeneous reaction rates, 2010 *Phys. Rev. E* **82** 051909.
- [8] Reichenbach T, Mobilia M, and Frey E. Mobility promotes and jeopardizes biodiversity in rock-paper-scissors games, 2007 *Nature* **448** 1046.
- [9] He Q, Täuber U C, and Zia R K P. On the relationship between cyclic and hierarchical three-species predator-prey systems and the two-species Lotka-Volterra model, 2012 *EPJ B* **85** 141.
- [10] Case S O, Durney C H, Pleimling M, and Zia R K P. Cyclic competition of four species: Mean-field theory and stochastic evolution, 2010 *EPL* **92** 58003.
- [11] Durney C H, Case S O, Pleimling M, and Zia R K P. Stochastic evolution of four species in cyclic competition, 2012 *J. Stat. Mech.* **2012** P06014.
- [12] Roman A, Konrad D, and Pleimling M. Cyclic competition of four species: domains and interfaces, 2012 *J. Stat. Mech.* **2012** P07014.
- [13] Zia R K P. General Properties of a System of S Species Competing Pairwise, 2010 *arXiv:1101.0018*.
- [14] Lotka A J. Undamped oscillations derived from the law of mass action, 1920 *J. Am. Chem. Soc.* **42** 1595.
- [15] Volterra V. Variazioni e fluttuazioni del numero d'individui in specie animali conviventi, 1926 *Mem. Accad. Sci. Lincei.* **2** 31.
- [16] Royama T. A comparative study of models for predation and parasitism, 1971 *Res Popul Ecol (Kyoto)* **13** 1.
- [17] Täuber U C. Population oscillations in spatial stochastic Lotka-Volterra models: a field-theoretic perturbational analysis, 2012 *J. Phys. A: Math. Theor.* **45** 405002.
- [18] Mobilia M, Georgiev I T, and Täuber U C. Phase Transitions and Spatio-Temporal Fluctuations in Stochastic Lattice Lotka-Volterra Models, 2007 *J. Stat. Phys.* **128** 447.
- [19] Washenberger M J, Mobilia M, and Täuber U C. Influence of local carrying capacity restrictions on stochastic predator-prey models, 2007 *J. Phys.: Condens. Matter* **19** 065139.
- [20] Haken H. *Synergetics*. Springer, New York, 3rd edition, 1983.
- [21] Rulands S, Zielinski A, Frey E. Global attractors and extinction dynamics of cyclically competing species, 2013 *Phys. Rev. E*, **87** 052710.
- [22] McKane A J and Newman T J. Predator-Prey Cycles from Resonant Amplification of Demographic Stochasticity, 2005 *Phys. Rev. Lett.* **94** 218102.
- [23] Dunbar S. Travelling wave solutions of diffusive Lotka-Volterra equations, 1983 *J. Math. Biol.* **17** 11.
- [24] He Q, Mobilia M, and Täuber U C. Coexistence in the two-dimensional May-Leonard model with random rates, 2011 *EPJ B* **82** 97.
- [25] Reichenbach T, Mobilia M, and Frey E. Self-organization of mobile populations in cyclic competition, 2008 *J. Theor. Biol.* **254** 368.
- [26] Mobilia M, Georgiev I T, and Täuber U. C. Fluctuations and correlations in lattice models for predator-prey interaction, 2006 *Phys. Rev. E* **73** 040903(R).
- [27] Kishida O, Mizuta Y, and Nishimura K. Reciprocal phenotypic plasticity in a predator-prey

- interaction between larval amphibians, 2006 *Ecology* **87** 1599–1604.
- [28] Yoshida T, Jones L E, Ellner S P, Fussmann G F, and Hairston N G. Rapid evolution drives ecological dynamics in a predator-prey system, 2003 *Nature* **424** 303.
 - [29] Fort H and Inchausti P. Biodiversity patterns from an individual-based competition model on niche and physical spaces, 2012 *J. Stat. Mech.* **2012** P02013.
 - [30] Rogers T, McKane A J, and Rossberg A G. Demographic noise can lead to the spontaneous formation of species, 2012 *EPL* **97** 40008.
 - [31] Traulsen A, Claussen J C, and Hauert C. Stochastic differential equations for evolutionary dynamics with demographic noise and mutations, 2012 *Phys. Rev. E* **85** 041901.
 - [32] Weitz J S, Hartman H, and Levin S A. Coevolutionary arms races between bacteria and bacteriophage, 2005 *Proc. Natl. Acad. Sci. USA* **102** 9535.
 - [33] Täuber U C, Howard M, and Vollmayr-Lee B P. Applications of field-theoretic renormalization group methods to reaction-diffusion problems, 2005 *J. Phys. A: Math. Gen.* **38** R79.
 - [34] Antal T and Droz M. Phase transitions and oscillations in a lattice prey-predator model, 2001 *Phys. Rev. E* **63** 056119.
 - [35] Parker M and Kamenev A. Extinction in the Lotka-Volterra model, 2009 *Phys. Rev. E* **80** 021129.
 - [36] Dobrinevski A and Frey E. Extinction in neutrally stable stochastic Lotka-Volterra models, 2012 *Phys. Rev. E* **85** 051903.